Inorganic Chemistry

Article

pubs.acs.org/IC

Exploring the Triplet Excited State Potential Energy Surfaces of a Cyclometalated Pt(II) Complex: Is There Non-Kasha Emissive Behavior?

Daniel Escudero* and Walter Thiel

Max-Planck-Institut für Kohlenforschung, Kaiser-Wilhelm-Platz 1, 45470 Mülheim an der Ruhr, Germany

Supporting Information

ABSTRACT: In this Article, we address the complexity of the emissive processes of a square-planar heteroleptic Pt(II) complex bearing 2-phenylpyridine (ppy) as cyclometalated ligand and an acetylacetonate derivative (dbm) as ancillary ligand. The origins of emission were identified with the help of density functional theory (DFT) and quadratic response (QR) time-dependent (TD)-DFT calculations including spin−orbit coupling (SOC). To unveil the photodeactivation mechanisms, we explored the triplet potential energy surfaces and computed the SOCs and the radiative decay rates (k_r) from possible emissive states. We find that emission likely originates from a higher-lying ^{3}MLCT/^{3}LLCT state and not from the Kasha-like ^{3}MLCT/^{3}LC$_{dbm}$ state. The temperature-dependent nonradiative deactivation mechanisms were also elucidated. The active role of metal-centered (^{3}MC) triplet excited states is confirmed for these deactivation pathways.

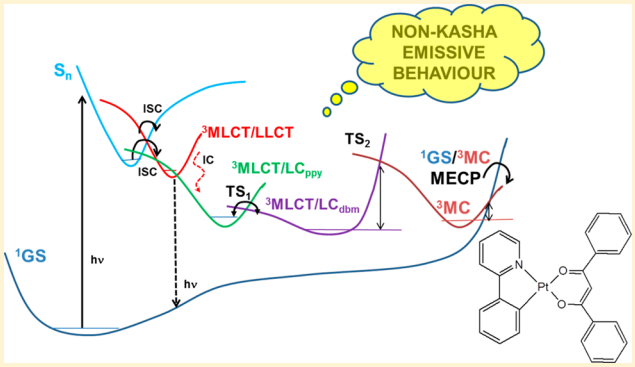

INTRODUCTION

Phosphorescent cyclometalated Pt(II) complexes have attracted much attention due to their potential application in light-emitting diodes,[1] sensor systems,[2] and biomedical imaging.[3] This is due to their outstanding optical properties, i.e., high photoluminescence efficiency, significant Stokes shifts, and tunable emission wavelengths and lifetimes.[4] All these properties make cyclometalated Pt(II) complexes excellent candidates for electroluminescence devices. The intense recent experimental activities on luminescent bidentate, tridentate, and tetradentate Pt(II) complexes[5] are not yet well-complemented by computational work. Although the calculation of the absorption spectra of such complexes is routine,[6] the computation and interpretation of their emissive properties remains more difficult. This is due to their intricate photophysical properties, characterized by a wide range of radiative decay rates and photoluminescence quantum yields. These observables are controlled by subtle variations of the electronic properties that are affected by spin−orbit and vibronic interactions, and there is a fine interplay of the effects of ligand substitution, medium (solution/solid), and temperature. This interplay may tune the radiative decay mechanisms arising from close-lying emissive triplet excited states, which often mix to a certain degree with singlet excited states. Recent computational studies on the emissive properties of Pt(II) complexes[6−8] pointed out that the emissive mechanisms are more complicated than expected, since the usual oversimplified picture of the lowest triplet excited state (T_1) being responsible for the radiative decay is far from realistic for such complexes.

Experimentally, using ligand design strategies, the photophysical properties of these complexes can be efficiently tuned. Ligand modification leads to shifts of the π/π^* and 5d(Pt) energy levels, which ultimately determine the energy of the singlet and triplet excited states. Thus, Pt(II) complexes with ligand-centered (LC)-,[9] mixed LC/metal-to-ligand charge-transfer (MLCT)-,[10] or mixed MLCT/ligand-to-ligand CT (LLCT)-based emission[11] have been reported in the literature. The character of the triplet excited state is the major factor governing the radiative decay rates. Another important goal in view of their potential applications is assuring photostability. Similarly to Ru(II)[12] and Ir(III)[13] complexes, nonemissive ^{3}MC states of Pt(II) complexes usually undergo nonradiative deactivation, which may ultimately impair their photostability, e.g., via ligand photodechelation. We and others have unveiled these pathways, which are also operative in Ru(II) and Ir(III) complexes.[14] These thermal nonradiative pathways compromise the photoluminescence quantum yields, since the nonradiative decay rates (k_{nr}'s) are increased. Concerning the radiative mechanisms in octahedral complexes, photoexcitation to a low-lying singlet excited state (S_n) is normally followed by very fast and efficient intersystem crossing (ISC) to the triplet manifold,[15] due to large spin−orbit couplings (SOCs).

Received: June 19, 2014
Published: October 7, 2014

However, for a series of Re(I) octahedral complexes, ISC rates were reported to be inversely proportional to the SOC constant of the ligand,[16] thus indicating the importance of vibronic couplings in these complexes. Ultrafast ISC processes were also found in square-planar cyclometalated Pt(II) complexes,[5] although in some particular cases fluorescence bands were also observed.[17]

According to the Kasha rule,[18] in the triplet manifold, there is fast decay to the lowest triplet excited state (T_1), from where emission likely occurs. The Kasha rule not only implies that the position of the emission maximum is independent of the excitation wavelength, but also that the quantum yield is also unaltered. The empirical Kasha rule was postulated at a time when lasers did not exist. In the decades since then, improvements in experimental techniques, i.e., ultrafast spectroscopies, enabled the observation of emissions from higher-lying molecular states, which represent "mild" violations of the Kasha rule as these emissive states are short-lived. In the past few years, several groups reported such examples for rhenium,[16] diplatinum,[19] and osmium[20] complexes, but also for organic neutral radicals,[21] the C_{70} molecule,[22] and some supramolecular complexes.[23]

To date, only few compounds have been identified that exhibit non-Kasha behavior at longer time scales. Among them, we highlight the organometallic (2-ferrocenyl)indene complex[24] and a Re(I)-bisthiazole complex.[25] The violation of the Kasha rule for these transition metal (TM) complexes has been attributed to photoisomerization reactions that lead to a mixture of isomers with different emission characteristics, which strictly speaking is not a violation of the Kasha rule but the consequence of a chemical reaction. For the Re(I) complex, this unusual behavior was experimentally corroborated by observing the emission wavelength to be dependent on the excitation wavelength. Another rather common feature in TM photochemistry is dual photoluminescence, with concomitant emission from thermally equilibrated excited states.[26] Several Pt(II) and Ir(III) cyclometalated complexes show this behavior.[17] A joint experimental and computational study of a dual phosphorescent Ir(III) complex[26a] found a low-lying ^{3}MLCT/^{3}LLCT and a high-lying ^{3}MLCT/^{3}LC excited state to be responsible for the emission spectra. At high temperatures the spectrum is dominated by the Kasha-type ^{3}MLCT/^{3}LLCT emission. However, at low temperatures interconversion between both states is thermally not allowed, since there is a considerable activation barrier for the ^{3}MLCT/^{3}LC → ^{3}MLCT/^{3}LLCT conversion. This prevents the relaxation to the lowest triplet state and thus breaches Kasha's rule. To summarize, there is not yet any published evidence for the violation of the Kasha rule at long time scales, which would neither be connected to photoisomerization nor to emission at low temperature. In this Article, we present a computational study of the triplet potential energy surfaces of a cyclometalated Pt(II) complex. We address the complexity of the emission processes and suggest on the basis of our computations that higher-lying emissive triplet states may be responsible for the photoluminescence at room temperature.

RESULTS AND DISCUSSION

Complex **1** (Chart 1) was synthesized and spectroscopically characterized by Gao et al.[27] Experimental data of complex **1** are collected in Table 1. The experimental emission spectrum shows a broad unstructured band from 400 to 650 nm with a maximum at ca. 465 nm. As reported in ref 27, the emissive characteristics of (ppy)Pt(acac) complexes are quite dependent on the nature of the ancillary ligand, ranging from broad unstructured emission bands to highly structured emission spectra. The recent improvements in quantum chemical methods for the excited states of TM complexes[28] extend the range of possible applications to a semiquantitative interpretation of their emission spectra.[29,30] To get insight into the emissive processes in complex **1** we explored its lowest triplet excited state potential energy surfaces (PES). Toward this aim, we determined the minimum geometries of the first eight triplet excited states at the TD-B3LYP level of theory. These TD-DFT optimized geometries served as an initial guess for the final UDFT (B3LYP/6-31G*) optimizations. For these calculations UDFT is preferred over TD-DFT, due to the problems of the latter to provide a balanced description of excited states of different character (especially if charge transfer states are involved).[31] With this protocol we were able to obtain the optimized geometries of four different triplet excited states (see below), whereas the optimizations for the other higher-lying triplet states failed due to variational collapse of the DFT calculation.

Chart 1. Chemical Structure of the Cyclometalated Pt(II) Complex 1

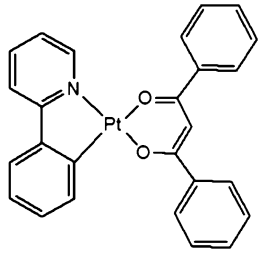

The geometries of the relevant fully optimized triplet excited state minima (^{3}MLCT/^{3}LC$_{ppy}$, ^{3}MLCT/^{3}LC$_{dbm}$, ^{3}MLCT/^{3}LLCT, and ^{3}MC) and of the ground state (^{1}GS) are shown in Figure 1. The assignment of the states is based on an analysis of their spin density distributions, which are also shown in Figure 1. The optimized structure of the lowest ^{3}MLCT/^{3}LC$_{ppy}$ state closely resembles the ^{1}GS geometry with regard to the square-planar coordination. It is characterized by a stronger binding of the ppy ligand, as reflected in the shorter Pt−N and Pt−C bond distances. The spin density is distributed among the ppy ligand and the Pt atom (amounting at the latter to 0.24, see Figure 1b), and hence points to its partial ^{3}MLCT character. The optimized geometry of the ^{3}MLCT/^{3}LC$_{dbm}$ state reveals larger displacements with respect to the ^{1}GS geometry. The square-planar coordination is partially distorted (see Figure 1c, dihedral angle ϕ_{NCPt1}), and the dbm ligand becomes strongly bound to the Pt atom. As a consequence, the ^{3}MLCT/^{3}LC$_{dbm}$ geometry contains larger C−O bond distances. The spin density is distributed on the dbm ligand and the Pt atom, in accordance with its character. The spin density at the Pt atom is 0.15, indicating a reduced ^{3}MLCT character as compared to the ^{3}MLCT/^{3}LC$_{ppy}$ state. The geometry of the higher-lying ^{3}MLCT/^{3}LLCT state (see Figure 1d) is similar to that of the ^{3}MLCT/^{3}LC$_{ppy}$ state with respect to the square-planar coordination of the Pt atom. The spin density is distributed among both ligands and the Pt atom, amounting at the latter to 0.37, in accordance to its mixed ^{3}MLCT/^{3}LLCT character. Thus, this state possesses the largest ^{3}MLCT

dx.doi.org/10.1021/ic501430x | Inorg. Chem. 2014, 53, 11015−11019

Table 1. Computed Adiabatic Energies, Emission Maxima, SOCs, and k_r Values from the Possible Emissive States

	^{3}MLCT/^{3}LC$_{dbm}$	^{3}MLCT/^{3}LC$_{ppy}$	^{3}MLCT/^{3}LLCT	expt
adiabatic relative energies: B3LYP/6-31G* (eV)	0.0	+0.114	+0.291	
ΔSCF-PCM(THF)- B3LYP/6-31G* [eV(nm)][a]	2.16 (573)	2.31 (536)	2.44 (508)	2.67 (465)
ΔSCF-B3LYP/6-31G* [eV(nm)]	2.15 (576)	2.29 (543)	2.58 (480)	
k_r ($T_{em} \rightarrow S_0$) [s^{-1}]	8.6	1.5	2.730×10^3	
SOCs ($T_{em} \rightarrow S_0$) (x-, y-, z-components) [cm^{-1}]	(−2.15, −1.56, −3.42)	(0.36, 0.94, 1.28)	(−3.20, −1.34, −0.58)	

[a]The PCM calculations were performed using THF as solvent.

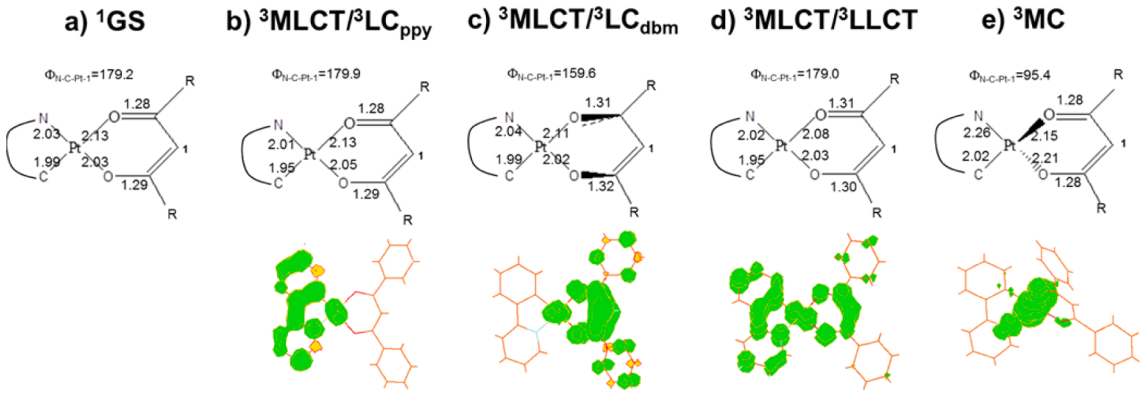

Figure 1. Selected bond lengths (Å) and angles (deg) in the optimized minimum structures of the ^{1}GS, ^{3}MLCT/^{3}LC$_{ppy}$, ^{3}MLCT/^{3}LC$_{dbm}$, ^{3}MLCT/^{3}LLCT, and ^{3}MC states of complex **1**. Computed spin density distributions (B3LYP/6-31G*) are shown below each triplet state.

character among all the possible emissive states. Finally, the geometry of the ^{3}MC state, which is a nonemissive state, shows the largest deviations from the ^{1}GS geometry, since the square-planar coordination is lost and the ligands become almost perpendicular to each other (see the dihedral angle ϕ_{NCPt1} of 95.4° in Figure 1e). Both the dbm and ppy ligands become less bound to the Pt atom, as reflected by the longer Pt−ligand bond distances. All these effects are caused by the promotion of an electron into the virtual $d_{x2-y2}\sigma^*$ orbital. The computed spin density at the Pt atom is 1.50, consistent with the metal-centered nature of this state.

We now address the origins of triplet emission of **1**. The phosphorescence emission maxima have been computed on the basis of ΔSCF-PCM-DFT calculations, which yield the energy difference between the lowest triplet excited state at its optimized geometry and the closed-shell ground state at the same geometry. This approach takes into account the geometrical and orbital relaxations upon photodeactivation. Moreover, the ΔSCF-PCM-DFT values (regardless of the system, the functional and whether they reach CT or local excitations) are more reliable than the corresponding singlet−triplet excitations from PCM-TD-DFT calculations,[32] due to the inherent problems of TD-DFT (see above). Table 1 lists the adiabatic energies and the ΔSCF-PCM-DFT values for the possible emissions from the ^{3}MLCT/^{3}LC$_{ppy}$, ^{3}MLCT/^{3}LC$_{dbm}$, and ^{3}MLCT/^{3}LLCT states. The ^{3}MLCT/LC$_{dbm}$ state is computed to be the lowest adiabatic emissive state, i.e., the Kasha state, being 0.114 eV (2.9 kcal/mol) below the ^{3}MLCT/LC$_{ppy}$ state. The higher-lying ^{3}MLCT/^{3}LLCT state is located 0.291 eV (6.7 kcal/mol) above the Kasha state. The phosphorescence emission maxima are calculated (ΔSCF-PCM-DFT) at 2.16, 2.31, and 2.44 eV for the ^{3}MLCT$_1$/^{3}LC$_{dbm}$, ^{3}MLCT/^{3}LC$_{ppy}$, and ^{3}MLCT/^{3}LLCT states, respectively. Table 1 also contains the gas-phase ΔSCF-DFT values, which indicate small hypsochromic shifts (blue shifts) for the first two states and a red shift of 0.14 eV for the ^{3}MLCT/^{3}LLCT emission. The computed ^{3}MLCT/^{3}LLCT emission maximum is closer to the experimental value of 2.67 eV (465 nm), being located 0.23 eV below the experimental value. Conversely, the ^{3}MLCT/^{3}LC$_{dbm}$ and ^{3}MLCT/^{3}LC$_{ppy}$ emission maxima are computed to be 0.51 and 0.36 eV below the experimental value. In view of the expected accuracy of the ΔSCF-PCM-DFT calculations (with root-mean-square deviations ranging from 0.25 to 0.5 eV for the electronic spectra of TM complexes[32]), our calculations point to a pool of several states that may be responsible for the emission characteristics of complex **1**. To get further insight into the emissive processes we have computed the k_r values of all possible emissive states at their optimized geometries using the QR TD-B3LYP approach (see Supporting Information).[33,34] The $k_r(T_{em} \rightarrow S_0)$ values and the corresponding SOCs($T_{em} \rightarrow S_0$) computed at the TD-B3LYP level are included in Table 1. The SOCs are quite small (a few cm^{-1}) for all emissive states because of their pronounced LC and LLCT character, and hence, the SO splittings and triplet−singlet admixtures are less pronounced than in the case of pure ^{3}MLCT states. The k_r values for emission from the ^{3}MLCT$_1$/^{3}LC$_{dbm}$ and ^{3}MLCT/^{3}LC$_{ppy}$ states are also very small, while the higher-lying emissive state, i.e., ^{3}MLCT/^{3}LLCT, has a larger k_r value, in accordance with previously reported results for similar Pt(II) complexes.[8] Since the SOCs and the emission energies are of similar order for all emissive states, we can attribute the difference in the k_r values to smaller vibronic couplings of the ^{3}MLCT$_1$/^{3}LC$_{dbm}$ and ^{3}MLCT/^{3}LC$_{ppy}$ states with the manifold of S_n and T_m states; i.e., the ^{3}MLCT/^{3}LLCT state borrows intensity more efficiently (see Supporting Information). Hence, it seems likely that the ^{3}MLCT/^{3}LLCT state is responsible of the emissive characteristics of complex **1**, since it has the largest computed k_r value and shows the best agreement of the computed emission energy with the experimental value (Table 1). Additionally, the experimental emission profile shows a less structured broad emission instead of a fine structure band that is typically observed for a ^{3}LC-

dx.doi.org/10.1021/ic501430x | Inorg. Chem. 2014, 53, 11015−11019

based emission; this also supports an emission with an increased amount of ^{3}MLCT character, in accordance with the calculations. However, we cannot exclude with certainty that other triplet states could also be responsible for the emission characteristics of complex **1**. Furthermore, in view of the observed broad emission profile (from 400 to 650 nm) it is conceivable that different emissive states may concomitantly contribute to the emission spectrum of **1**. In a nutshell, our calculations favor non-Kasha behavior of photoluminescence in this Pt(II) complex, but further experimental evidence is required to confirm this hypothesis.

We now propose an explanation of the complete photodeactivation mechanism in **1**. A schematic Jablonski diagram is shown in Figure 2, which includes the optimized triplet excited

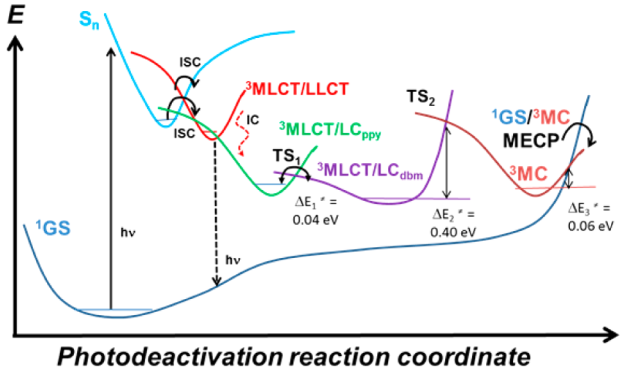

Figure 2. Schematic Jablonski diagram of complex **1**, including the lowest-energy states involved in the proposed radiative and nonradiative deactivation pathways.

state minima. We additionally optimized the geometries of the relevant transition states and of a minimum-energy crossing point (^{1}GS/^{3}MC MECP) along the photodeactivation reaction coordinate. TS$_1$ and TS$_2$ are the transition states for the ^{3}MLCT/^{3}LC$_{ppy}$ → ^{3}MLCT/^{3}LC$_{dbm}$ and ^{3}MLCT/^{3}LC$_{dbm}$ → ^{3}MC conversions, respectively. The main geometrical features of these species are highlighted in Figure 3. The TS$_1$ geometry

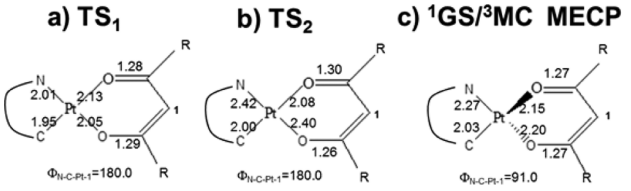

Figure 3. Selected bond lengths (Å) and angles (deg) of the TS$_1$ (a), TS$_2$ (b), and ^{1}GS/^{3}MC MECP (c) structures of complex **1**.

closely resembles the ^{3}MLCT/^{3}LC$_{ppy}$ geometry. Its imaginary mode involves the wagging of the dbm ligand (50i cm^{-1}) indicating that TS$_1$ belongs to the ^{3}MLCT/^{3}LC$_{ppy}$ → ^{3}MLCT/^{3}LC$_{dbm}$ deactivation pathway. Unlike the ^{3}MC minimum, the TS$_2$ geometry still has a square-planar coordination. At the TS$_2$ geometry (see Figure 3), most of the Pt−ligand bond distances are stretched, some of them even more than at the ^{3}MC geometry, due to the partial population of the $d_{x2-y2}\sigma^*$ orbital. The spin density at the Pt atom (1.32) and the nature of the imaginary mode (ppy twist, 30i cm^{-1}) show that this transition state belongs to the ^{3}MLCT/^{3}LC$_{dbm}$ → ^{3}MC deactivation pathway. The ^{1}GS/^{3}MC MECP geometry is close to the ^{3}MC minimum geometry (see Figure 3). The spin density at the Pt atom (1.48) confirms the active role of the ^{3}MC state on the thermal nonradiative deactivation pathways.

Upon irradiation (experiment: 313 nm, 3.97 eV),[27] the singlet manifold (S$_n$) is populated. From there, ultrafast ISCs will lead to the triplet manifold. Thus, as schematically shown in Figure 2, the different emissive states will be populated in a competitive way. Due to the larger radiative rate from the higher-lying ^{3}MLCT/^{3}LLCT state (as compared to the other triplet states), radiative drainage will preferentially occur from this state. Internal conversion (IC) processes via vibrational relaxation and solvent reorganization will populate the low-lying ^{3}MLCT/^{3}LC$_{ppy}$ and ^{3}MLCT/^{3}LC$_{dbm}$ states. Interconversion between these two states is facile, since the barrier between them is only ca. 0.04 eV (1 kcal/mol), see $\Delta E_1^{\ddagger}$ in Figure 2.

After disentangling the radiative processes, we address the thermally activated nonradiative photodeactivation mechanism. We note that, in a recent study on tetradentate Pt(II) square-planar complexes, the simple energy gap law was found insufficient to account for the global nonradiative decay rates.[35] As shown in Figure 2, the rate-determining step for the nonradiative pathways in complex **1** is the population of the ^{3}MC well via the TS$_2$ structure, which lies 0.40 eV (9.3 kcal/mol) above the ^{3}MLCT/^{3}LC$_{dbm}$ minimum. Thereafter, the ^{1}GS/^{3}MC surface crossing point is easily accessible, being located at 0.06 eV (1.3 kcal/mol) above the ^{3}MC minimum. This is the most important funnel for the photodeactivation of complex **1**. Thus, if enough vibrational energy is available, the system will be able to surmount these barriers and readily decay to the ground state. The proximity of the ^{1}GS/^{3}MC MECP structure to the ^{3}MC minimum assures the high photostability of complex **1**. Hence, once the ^{1}GS/^{3}MC MECP is passed, the molecule will relax to the S$_0$ geometry. The ease of this process harms the photoluminescence quantum yields, in line with the experimental finding of rather low quantum yields at room temperature (ca. 2%).[27]

Generally speaking, the photoluminescence quantum yield is governed not only by the thermally dependent nonradiative rate, but also by the radiative and the thermally independent nonradiative rates, which all need to be analyzed to evaluate the quantum yield. We note in this context that the barriers to populate ^{3}MC states of octahedral Ir(III) cyclometalated complexes are normally larger than those computed here for complex **1**,[14b] in agreement with the observed larger quantum yields for Ir(III) complexes as compared to square-planar Pt(II) cyclometalated complexes. In addition, the k_r values are generally larger for octahedral Ir(III) complexes than for square-planar Pt(II) complexes.[5]

■ CONCLUSIONS

Summarizing, this computational work demonstrates intricate emissive processes in complex **1**, with several low-lying triplet excited states that may be responsible for its emissive features. We have considered deactivation processes involving four triplet excited states. The available experimental and computational evidence favors non-Kasha emissive behavior of complex **1**, but further experimental work is needed to confirm this suggestion, which goes beyond the commonly accepted notions on the photophysics of TM complexes at long time scales. We anticipate that the conclusions of the present work may be transferable to other TM complexes, e.g., to explain the counterintuitive emissive behavior in other Pt(II) cyclo-

dx.doi.org/10.1021/ic501430x | Inorg. Chem. 2014, 53, 11015−11019

metalated complexes.[36] Furthermore, we have disentangled the thermally activated nonradiative deactivation pathways of complex **1**. The photostability of this complex has been rationalized considering the key role of a ^{1}GS/^{3}MC MECP structure, which lies close to the ^{3}MC minimum and provides a facile pathway back to the ground state, thus preventing other undesirable photoreactions.

■ ASSOCIATED CONTENT

Ⓢ Supporting Information

Computational details and Cartesian coordinates of the optimized geometries. This material is available free of charge via the Internet at http://pubs.acs.org.

■ AUTHOR INFORMATION

Corresponding Author

*E-mail: escudero@kofo.mpg.de.

Notes

The authors declare no competing financial interest.

■ REFERENCES

(1) (a) Kalinowski, J.; Fattori, V.; Cocchi, M.; Williams, J. A. G. *Coord. Chem. Rev.* **2011**, *255*, 2401−2425. (b) Kwok, C.-C.; Ngai, H. M. Y.; Chan, S.-C.; Sham, I. H. T.; Che, C.-M.; Zhu, N. *Inorg. Chem.* **2005**, *44*, 4442−4444.

(2) (a) Wong, K. M.-C.; Tang, W.-S.; Lu, X.-X.; Zhu, N.; Yam, V. W.-W. *Inorg. Chem.* **2005**, *44*, 1492−1498. (b) Evans, R. C.; Douglas, P.; Williams, J. A. G.; Rocheste, D. L. *J. Fluoresc.* **2006**, *16*, 201−206. (c) Karakus, C.; Fischer, L. H.; Schmeding, S.; Hummel, J.; Risch, N.; Schäferling, M.; Holder, E. *Dalton Trans.* **2012**, *41*, 9623−9632.

(3) Mou, X.; Wu, Y.; Liu, S.; Shi, M.; Liu, X.; Wang, C.; Sun, S.; Zhao, Q.; Zhou, X.; Huang, W. *J. Mater. Chem.* **2011**, *21*, 13951−13962.

(4) Williams, J. A. G. *Top. Curr. Chem.* **2007**, *281*, 205−268.

(5) See: Rausch, A. F.; Homeier, H. H. H.; Yersin, H. *Top. Organomet. Chem.* **2010**, *29*, 193−235 and references therein.

(6) Gourlaouen, C.; Daniel, C. *Dalton Trans* **2014**, DOI: 10.1039/c4dt01822b.

(7) Tong, G. S. M.; Che, C.-M. *Chem.—Eur. J.* **2009**, *15*, 7225−7237.

(8) Lam, W. H.; Lam, E. S.-H.; Yam, V. W.-W. *J. Am. Chem. Soc.* **2013**, *135*, 15135.

(9) Liu, R.; Chen, H.; Chang, J.; Li, Y.; Zhu, H.; Sun, W. *Dalton Trans.* **2013**, *42*, 160−171.

(10) Wu, W.; Wu, W.; Ji, S.; Gui, H.; Zhao, J. *Eur. J. Inorg. Chem.* **2010**, 4470−4482.

(11) Mou, X.; Wu, Y.; Liu, S.; Shi, M.; Liu, X.; Wang, C.; Sun, S.; Zhao, Q.; Zhiu, X.; Huang, W. *J. Mater. Chem.* **2011**, *21*, 13951−13962.

(12) (a) Marin, V.; Holder, E.; Hoogenboom, R.; Schubert, U. S. *Chem. Soc. Rev.* **2007**, *36*, 618−635. (b) Escudero, D.; Happ, B.; Winter, A.; Hager, M. D.; Schubert, U. S.; González, L. *Chem.—Asian J.* **2012**, *7*, 667−671.

(13) Tian, N.; Lenkeit, D.; Pelz, S.; Fischer, L. H.; Escudero, D.; Schiewek, R.; Klink, D.; Schmitz, O. J.; González, L.; Schäferling, M.; Holder, E. *Eur. J. Inorg. Chem.* **2010**, *30*, 4875−4885.

(14) (a) Heully, J.-L.; Alary, F.; Boggio-Pasqua, M. *J. Chem. Phys.* **2009**, *131*, 184308. (b) Escudero, D.; Heuser, E.; Meier, R. J.; Schäferling, M.; Thiel, W.; Holder, E. *Chem.—Eur. J.* **2013**, *19*, 15639−15644.

(15) (a) Canizzo, A.; van Mourik, F.; Gawelda, W.; Zgrablic, G.; Bressler, C.; Chergui, M. *Angew. Chem., Int. Ed.* **2006**, *45*, 3174−3176. (b) Bhasikuttan, A. C.; Suzuki, M.; Nakashima, S.; Okada, T. *J. Am. Chem. Soc.* **2002**, *124*, 8398−8405. (c) Hedley, G. J.; Ruseckas, A.; Samuel, I. D. W. *J. Phys. Chem. A* **2009**, *113*, 2.

(16) Canizzo, A.; Blanco-Rodríguez, A. M.; El Nahhas, A.; Sebera, J.; Zalis, S.; Vlcek, A., Jr.; Chergui, M. *J. Am. Chem. Soc.* **2008**, *130*, 8967−8974.

(17) Kozhevnikov, D.; Kozhevnikov, V. N.; Shafikov, M. Z.; Prokhorov, A. M.; Bruce, D. W.; Gareth Williams, J. A. *Inorg. Chem.* **2011**, *50*, 3804−3815.

(18) Kasha, M. *Discuss. Faraday Soc.* **1950**, *9*, 14−19.

(19) van der Veen, R. M.; Canizzo, A.; van Mourik, F.; Vlcek, A., Jr.; Chergui, M. *J. Am. Chem. Soc.* **2011**, *133*, 305−315.

(20) Bräm, O.; Messina, F.; Baranoff, E.; Canizzo, A.; Nazeeruddin, M. K.; Chergui, M. *J. Phys. Chem. C* **2013**, *117*, 15958−15966.

(21) Sakamoto, M.; Cai, X.; Hara, M.; Tojo, S.; Fujikutsa, M.; Majima, T. *J. Am. Chem. Soc.* **2005**, *127*, 3702−3703.

(22) Sassara, A.; Zerza, G.; Chergui, M. *J. Phys. Chem. A* **1998**, *102*, 3072−3077.

(23) Yanagi, K.; Kataura, H. *Nat. Photonics* **2010**, *4*, 200−201.

(24) Scuppa, S.; Orian, L.; Donoli, A.; Santi, S.; Meneguetti, M. *J. Phys. Chem. A* **2011**, *115*, 8344−8349.

(25) Henry, K. E.; Balasingham, R. G.; Vortherms, A. R.; Platts, J. A.; Valliant, J. F.; Coogan, M. P.; Zubieta, J.; Doyle, R. P. *Chem. Sci.* **2013**, *4*, 2490−2495.

(26) (a) Yeh, Y.-S.; Cheng, Y.-M.; Chou, P.-T.; Lee, G.-H.; Yang, C.-H.; Chi, Y.; Shu, C.-F.; Wang, C.-H. *ChemPhysChem* **2006**, *7*, 2294−2297. (b) Lo, K. K-W.; Zhang, K. Y.; Leung, S.-K.; Tang, M.-C. *Angew. Chem., Int. Ed.* **2008**, *47*, 2213−2216. (c) Ladouceur, S.; Donato, L.; Romain, M.; Mudraboyina, B. P.; Johansen, M. B.; Wisner, J. A.; Zysman-Colman, E. *Dalton Trans.* **2013**, *42*, 8838−8847.

(27) Liu, J.; Yang, C-J.; Cao, Q-.Y.; Xu, M.; Wang, J.; Peng, H-.N.; Tan, W-.F.; Lü, X-.X.; Gao, X-.C. *Inorg. Chim. Acta* **2009**, *362*, 575−579.

(28) (a) González, L.; Escudero, D.; Serrano-Andrés, L. *ChemPhysChem* **2012**, *13*, 28−51. (b) Daniel, C. *Coord. Chem. Rev.* **2014**, DOI: 10.1016/j.ccr.2014.05.023.

(29) (a) Li, X.; Minaev, B.; Ågren, H.; Tian, H. *J. Phys. Chem. C* **2011**, *115*, 20724−20731. (b) Jansson, E.; Minaev, B.; Schrader, S.; Ågren, H. *Chem. Phys.* **2007**, *333*, 157. (c) Sousa, C.; de Graaf, C.; Rudavskyi, A.; Broer, R.; Tatchen, J.; Etinski, M.; Marian, C. M. *Chem.—Eur. J.* **2013**, *19*, 17541−17551.

(30) Minaev, B.; Baryshnikov, G.; Agren, H. *Phys. Chem. Chem. Phys.* **2014**, *16*, 1719−1758.

(31) Escudero, D.; Thiel, W. *J. Chem. Phys.* **2014**, *140*, 194105.

(32) Zhekova, H. R.; Seth, M.; Ziegler, T. *Int. J. Quantum Chem.* **2014**, *114*, 1019−1029.

(33) (a) Vahtras, O.; Agren, H.; Jorgensen, J.; Jense, H. J. A.; Helgaker, T.; Olsen, J. *J. Chem. Phys.* **1992**, *97*, 9178. (b) Olsen, J.; Jorgensen, P. *J. Chem. Phys.* **1985**, *82*, 3235. (c) Casida, M. *THEOCHEM.* **2009**, *914*, 3.

(34) (a) Minaev, B.; Ågren, H. *Chem. Phys.* **2005**, *315*, 215−239. (b) Li, X.; Minaev, B.; Ågren, H.; Tian, H. *Eur. J. Inorg. Chem.* **2011**, *2011*, 2517−2524.

(35) Tong, G. S. M; Chow, P. K.; To, W.-P.; Kwok, W.-M.; Che, C.-M. *Chem.—Eur. J.* **2014**, *20*, 6433−6443.

(36) Bossi, A.; Rausch, A. F.; Leitl, M. J.; Czerwieniec, R.; Whited, M. T.; Djurovich, P. I.; Yersin, H.; Thompson, M. E. *Inorg. Chem.* **2013**, *52*, 12403−12415.